

Olivier Beyssac · Jean-Noël Rouzaud · Bruno Goffé  
Fabrice Brunet · Christian Chopin

## Graphitization in a high-pressure, low-temperature metamorphic gradient: a Raman microspectroscopy and HRTEM study

Received: 9 February 2001 / Accepted: 15 October 2001 / Published online: 8 February 2002  
© Springer-Verlag 2002

**Abstract** The graphitization of carbonaceous material (CM) in a high-pressure metamorphic gradient is characterized along a cross section in the Schistes Lustrés formation, Western Alps. Along this 25-km cross section, both the CM precursor and the host-rock lithology are homogeneous, and the prograde evolution of the pressure–temperature metamorphic conditions from the lower blueschist-facies (13 kbar, 330 °C) to the eclogite-facies (20 kbar, 500 °C) is tightly constrained by literature data. Raman microspectroscopy shows that at the micrometre scale, this process is progressive and continuous with increasing metamorphic grade, and that the structure of CM is very sensitive to temperature variations. At the nanometre scale (HRTEM), the CM is composed of a mixture of a microporous phase and an onion-ring like phase, both known as non-graphitizing under the effect of temperature at ambient pressure. The HP–LT graphitization produces structurally and microtexturally heterogeneous CM. With increasing metamorphic grade, the graphitization of the two types of CM proceeds up to the triperiodic graphite stage because of microtextural and structural changes that are specific to each type of CM. The microporous material is progressively transformed into graphite through a macroporous transitional stage. In this case, graphitization mainly occurs on the pore walls as a result of pore growth. In the case of concentric onion-ring like mate-

rial, graphitization occurs in the regions with the largest radius of curvature, i.e. on the outer part of the ring. In comparison with 1-bar experiments, pressure seems to induce microtextural changes, which allows the subsequent structural modifications of the starting material.

### Introduction

Carbonaceous material (CM) is widespread in metamorphic rocks, especially metasedimentary ones. This CM derives from the conversion during the diagenetic and metamorphic processes of organic matter originally present in the host sedimentary rock. This transformation, which is called graphitization, proceeds through a series of intermediate forms and, locally, can reach the triperiodic graphite structure. The transformation from short and misorientated aromatic layers in poorly organized CM up to perfectly stacked layers in the triperiodic structure of graphite is achieved by microtextural, structural, and chemical modifications of the starting material. During the aromatic layers growth and stacking improvement, both compositional and organizational changes are involved in the graphitization process. As a consequence, the graphitization degree strongly depends on both composition and organization of the starting material (Bény-Bassez and Rouzaud 1985; Rouzaud and Oberlin 1989; Kribek et al. 1994; Large et al. 1994; Bustin et al. 1995; Beyssac et al. 2000).

In industrial processes, synthesis of graphite needs a graphitizing precursor (lamellar precursor) and a temperature of 2,800 °C (Rouzaud and Oberlin 1989) whereas, in the natural context, all types of precursors are transformed into graphite at a temperature close to 450–500 °C (Wang 1989). In the material-sciences field, the study of graphitization of synthetic carbon precursors heat-treated under pressure has shown that non-lamellar precursors, which are not graphitizing under the effect of temperature at ambient pressure, could graphitize by adding hydrostatic or oriented pressures

O. Beyssac (✉) · B. Goffé · F. Brunet · C. Chopin  
Laboratoire de Géologie, CNRS-UMR 8538,  
Ecole Normale Supérieure, 24 rue Lhomond,  
75231 Paris Cedex 05, France  
E-mail: olivier.beyssac@ens.fr  
Tel.: +33-1-44322275  
Fax: +33-1-44322000

J.N. Rouzaud  
Centre de Recherche sur la Matière Divisée,  
UMR 6619, CNRS-Université d'Orléans,  
1b rue de la Férellerie,  
45071 Orléans Cedex 2, France

Editorial responsibility: J. Hoefs

(De Fonton et al. 1980; Bustin et al. 1995; Beyssac et al. 2000). As a consequence, it is generally considered that natural graphitization is controlled mainly by temperature with additional influences of pressure, duration of the metamorphic event and shear strain (Landis 1971; Diessel et al. 1978; Bonijoly et al. 1982; Wopenka and Pasteris 1993; Wada et al. 1994; Bustin et al. 1995; Suchy et al. 1997). Nevertheless, the respective influences of those parameters have never been quantitatively assessed.

Several authors have studied CM in metamorphic rocks by using X-ray diffraction (XRD; Landis 1971; Grew 1974; Diessel et al. 1978; Itaya 1981; Wada et al. 1994; Nishimura et al. 2000), high-resolution transmission electron microscopy (HRTEM; Bonijoly et al. 1982; Goffé and Villey 1984; Buseck and Huang 1985; Deurbergue et al. 1987; Buseck et al. 1988; Jehlicka and Rouzaud 1989; Large et al. 1994; Kovalevski et al. 2001), reflectance measurements (Okuyama-Kusunose and Itaya 1987; Suchy et al. 1997) or Raman microspectroscopy (Pasteris and Wopenka 1991; Wopenka and Pasteris 1993; Kribek et al. 1994; Yui et al. 1996; Jehlicka and Rouzaud 1997). Both Raman microspectroscopy and XRD provide quantitative parameters on the degree of organization of CM, but because of a higher spatial resolution ( $\mu\text{m}^3$  vs  $\text{mm}^3$ ), Raman microspectroscopy gives less averaged information. For that reason, and because Raman microspectroscopy can be performed within thin sections and thus does not require the extraction of CM from the host rock like XRD, it is now commonly assumed that Raman microspectroscopy is more appropriate than XRD in the study of CM from metamorphic rocks (Wopenka and Pasteris 1993). HRTEM investigations are fundamental to obtain information about both the structure (organization at the atomic scale of the layers, either isolated or stacked to form basic structural units – BSU) and the microtexture (mutual orientation in space of the layers). The combination of HRTEM and Raman microspectroscopy, thus, is very promising because Raman microspectroscopy gives the quantitative parameters that are difficult, and even impossible, to obtain from HRTEM pictures with such heterogeneous materials. Nevertheless, although both methods have been used in the study of synthetic carbons (Bény-Bassez and Rouzaud 1985) or in the study of the alteration of graphite in a uranium deposit (Wang et al. 1989), the two methods have been rarely used together in the study of metamorphic CM. Only Wopenka and Pasteris (1993) have analysed with Raman microspectroscopy some of the samples previously investigated using HRTEM (Buseck and Huang 1985).

All the studies cited above have focused on CM issued from natural samples submitted to high-temperature, low-pressure (HT–LP) metamorphic gradients, except Diessel et al. (1978) and Itaya (1981) who looked at the high-pressure schists from New Caledonia and Japan, respectively, both using XRD. It is important to note that in all of these studies the degree of organization of CM is compared with metamorphic grade as

grossly defined by index minerals with broad P–T stability fields (chlorite, biotite and garnet for instance), but is never correlated directly with precise metamorphic pressure and temperature determinations.

The aim of this study, thus, is to document the natural graphitization process under pressure and to characterize the mechanisms of transformation in this particular case. In the following, we characterize the graphitization process of CM submitted to high-pressure, low-temperature (HP–LT) metamorphism by coupling Raman microspectroscopy and HRTEM. We have chosen a geological cross section in the Schistes Lustrés unit, Western Alps, where geological, metamorphic and tectonic parameters are well constrained (Agard et al. 2001a, 2001b). Moreover, in this homogeneous series, the duration of the unique metamorphic event can be considered as equal for all samples and the type of organic precursor is the same all along the cross section. These two conditions are fundamental for the interpretation of the results, but were not fulfilled in most previous studies. We define here a starting material in the lowest grade sample, and we characterize the mechanism of graphitization and quantify the associated organizational modifications of such a material as a result of increasing metamorphic grade.

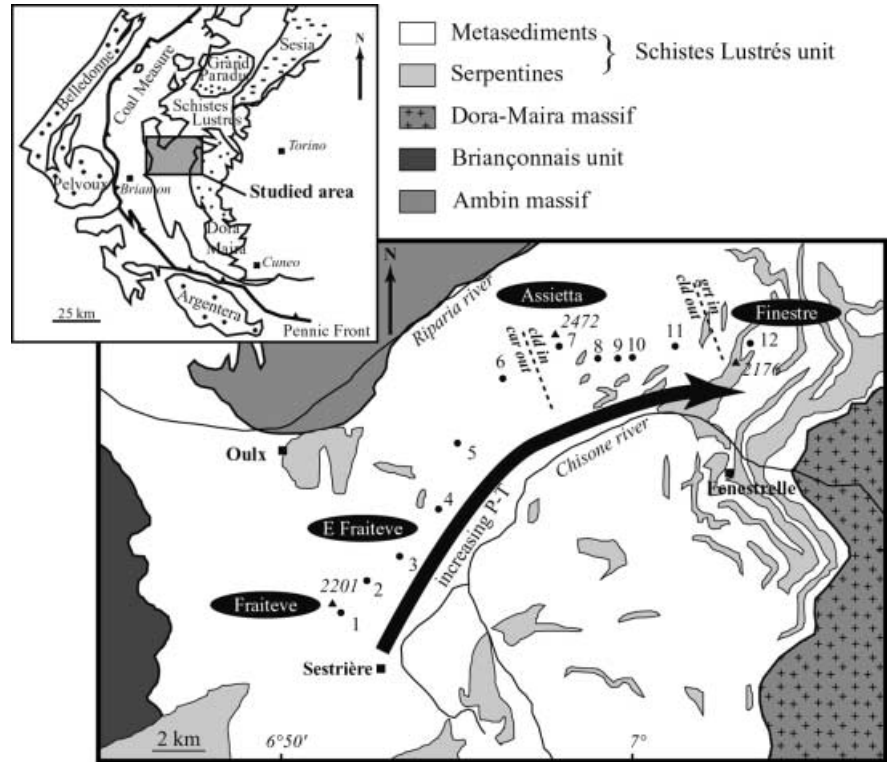
---

## Geological background and sample selection

The Western Alps are one of the reference belts in the study of HP–LT metamorphism. The degree of metamorphism varies from lower greenschist facies in the external zones up to ultra-high pressure eclogitic conditions in the Dora-Maira massif (Michard et al. 1996). The Schistes Lustrés unit belongs to the Liguro–Piemontese domain, which is derived from the Alpine branch of the Tethys ocean and represents now a 20-km wide, 200-km long and 10–15 km thick unit. The oceanic Schistes Lustrés unit is mainly composed of calc-schists and black-schists from the Malm to the Senonian (Caron 1977; Barfety et al. 1995), including large ophiolitic lenses. This unit is bordered by relics of the European palaeomargins: the low-grade high-pressure Briançonnais units to the west and the ultra high-pressure Dora-Maira massif to the east. The Schistes Lustrés unit, thus, is a transitional zone presenting a metamorphic gradient between those extremes. The whole region is supposed to result from east–southward subduction of the European continent under the Apulian margin followed by collision (Michard et al. 1996; Stampfli and Marchant 1997). Agard et al. (2001a, 2001b) showed that the tectono-metamorphic evolution of the Schistes Lustrés is made of successive episodes that are between 55 and 35 million years old. Along the selected cross section, the duration of the metamorphic event, thus, can be taken as constant equal to about 20 million years.

In this study, we chose to focus on a well-studied cross section between the Fraiteve Mount and the Finestre Pass, close to Sestrière in Italy (Fig. 1). Both the

**Fig. 1.** Geological map of the Schistes Lustrés unit in the studied area. Sample location and the main mineral isograds are represented. *car* Carpholite; *clt* chloritoid; *grt* garnet (after Agard et al. 2001a, 2001b). Minerals abbreviations after Kretz (1983)



tectonic and metamorphic evolutions along this cross section have been studied in detail by Agard et al. (2001a, 2001b). This section presents continuous outcrops along its 25-km length from the external part (Fraiteve Mount) to the most internal part (Finestre Pass) of the Schistes Lustrés unit. Along this section, the lithology is mainly composed of calc-schists with locally interlayered metabasite and serpentinite boudins. The mineral matrix is mainly constituted by quartz, calcite, phengite, paragonite, chlorite and metamorphic index minerals (Fe–Mg carpholite, lawsonite, chloritoid and garnet). In Fig. 1, we have represented the location of the main isograds for these index minerals. The pressure–temperature (P–T) conditions have been estimated by Agard et al. (2001a, 2001b) using the presence of index minerals and multi-equilibrium thermobarometry (Fig. 2). These conditions vary from the lower blueschist facies (13 kbar, 330 °C in Fraiteve) up to the eclogitic facies (20 kbar, 500 °C in Finestre) as is shown in Fig. 2. Thus, the metamorphic evolution in the Schistes Lustrés unit is typical of a HP–LT gradient ( $\sim 10$  °C/km), in contrast to previous studies that have focused on HT–LP samples (30–40 °C/km, Buseck and Huang 1985; Wopenka and Pasteris 1993; Yui et al. 1996) as represented in Fig. 2.

CM is present along the whole cross section and represents less than 1 wt% of the host rock, on average. These black schists, comparable to the Atlantic Apto-Albian black shales described by Lemoine et al. (1986), constitute part of a detrital deep-water formation. CM was diffuse in the starting material and the type of carbon precursor should be an algae kerogen type II

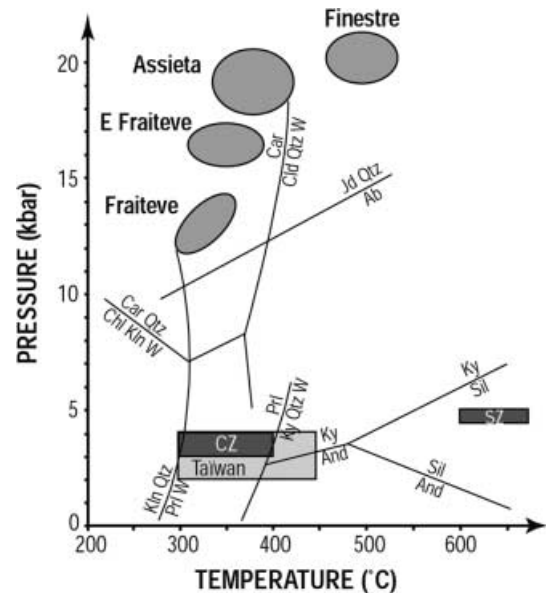


**Fig. 2.** P–T diagram relevant to the geological cross section. The P–T estimates for the studied samples are reported according to Agard et al. (2001a, 2001b). We have also represented the P–T conditions for the HT–LP samples studied by Buseck and Huang (1985) and later by Wopenka and Pasteris (1993; CZ chlorite zone; SZ sillimanite zone) and Yui et al. (1996; Taiwan). Minerals abbreviations after Kretz (1983)

(Durand and Monnin 1980) from Tethyan sediments. During the metamorphic process, CM was segregated from the silicate and carbonate matrix and now occurs as beds, underlining the tectonic foliation at micrometre

to centimetre scale. We selected 12 samples equally distributed along the cross section (Fig. 1), from a low-grade blueschist (sample 1) to eclogitic conditions (Fig. 2, sample 12). This sampling is representative of the whole P–T evolution along the cross section. From a tectonic point of view, the cross section is characterized by large gradients of deformation from less deformed gently foliated zones to major ductile shear zones (Agard et al. 2001a, 2001b). We chose samples from both types of zones to check the possible influence of shear on the graphitization process in a metamorphic context.

## Sample preparation and analytical methods

### Sample preparation

Given the low CM content of the samples (< 1 wt%), it was necessary to extract CM from the host rock for the HRTEM investigations. About 15–25 g of rocks were ground during a few tens of minutes and then CM was extracted from the whole rock by dissolution of silicate and carbonate phases by HF and HCl. We assumed that such a short mechanical grinding had no effect on CM. As demonstrated by Salver-Disma et al. (1999), mechanical grinding damages the CM structure (graphite and various synthetic cokes were tested in their study) after durations of more than 20 h. Rock powders were firstly attacked by 11 N HCl and then by a mixture of one-third 11 N HCl and two-thirds 23 N HF at a temperature around 80 °C. Finally, CM was washed with HCl to remove part of the sulfides and with hot pure water. In the CM residue, some minerals such as pyrite and zircon have been found. More surprisingly, we also observed very small micas, which were totally embedded in CM (for instance phengites were characterized by EDX microanalysis). Therefore, we did not perform chemical elemental analysis for this study because the contribution of these hydrated minerals to such analysis is certainly not negligible, as discussed by Wang (1989).

A few milligrams of the extracted CM were dispersed by ultrasounds in anhydrous ethanol after grinding by hand in a small agate mortar. A drop of this suspension was then deposited on a TEM grid covered by a holey amorphous carbon film. Observations were carried out on the thinnest fragments placed across the holes. The holey grid was used to reduce the background noise caused by the amorphous supporting film, and also to check the possible presence of an amorphous phase.

Raman spectra were recorded on thin sections. Numerous authors have raised the problem of the possible damage effects caused to the CM structure by the making thin-sections and polishing (Pasteris 1989; Mostefaoui et al. 2000) or mechanical milling (Salver-Disma et al. 1999). In order to avoid any mechanical disruption of CM, we chose to focus the laser on CM situated beneath the surface of a transparent adjacent grain, as suggested by Pasteris (1989). Moreover, as the Raman spectrum of CM is sensitive to the orientation of CM with respect to the incident laser beam (Wang et al. 1989), we chose to cut all the thin sections perpendicular to the foliation and, thus, the optical axis of the laser beam was set perpendicular to the graphite mean *c*-axis orientation (Kribek et al. 1994).

### Raman spectroscopy

We used a Dilor XY double subtractive spectrograph with premonochromator, equipped with confocal optics before the spectrometer entrance, and a nitrogen-cooled SPECTRUM1 CCD detector (Jobin Yvon). A microscope was used to focus the excitation laser beam (514.5-nm exciting line of a Spectra Physics Ar<sup>+</sup> laser) on the sample and to collect the Raman signal in the back-scattered direction. The presence of the confocal pinhole before the spectrometer entrance ensures a sampling of a 2–4- $\mu$ m sized zone

with a 50 $\times$  objective, with a final laser power of about 1–5 mW at the sample surface. Acquisition time was 20–300 s and 15–20 spectra were recorded for each sample. Peak position band area (i.e. integrated area) and band width (i.e. full width at half maximum, FWHM) were determined using the computer program PeakFit 3.0 (Jandel Scientific). An example of decomposition obtained with the fitting procedure is presented in Fig. 3.

The Raman spectrum of CM can be divided in first- and second-order regions (Tuinstra and Koenig 1970; Nemanich and Solin 1979; Ferrari and Robertson 2000). In the first-order region (1,100–1,800 cm<sup>-1</sup>, Fig. 3), the E<sub>2g2</sub> vibration mode of graphite with D<sub>6h</sub><sup>4</sup> crystal symmetry occurs at  $\sim$ 1,580-cm<sup>-1</sup> (G band). For poorly organized CM, additional bands appear in the first-order region at  $\sim$ 1,150,  $\sim$ 1,350,  $\sim$ 1,500- and  $\sim$ 1,620-cm<sup>-1</sup>. The 1,150-cm<sup>-1</sup> component appears only in very poorly organized CM. The 1,350-cm<sup>-1</sup> band (D1 band), commonly called the defect band, has been attributed to in-plane defects and heteroatoms (Bény-Bassez and Rouzaud 1985). Its characteristics (i.e. integrated area, FWHM, intensity) as compared with those of the G band, are commonly used as quantitative parameters of the graphitization process (Tuinstra and Koenig 1970; Lespade et al. 1984; Bény-Bassez and Rouzaud 1985; Wopenka and Pasteris 1993; Yui et al. 1996). The 1,500-cm<sup>-1</sup> band (D3 band), which appears only as a very wide band in poorly crystallized CM, has been attributed by Bény-Bassez and Rouzaud (1985) to defects outside the plane of aromatic layers such as tetrahedral carbons. At last the 1,620-cm<sup>-1</sup> band (D2 band) makes a shoulder on the G band. In perfect graphite this component is absent, whereas in very poorly organized CM, the G and D2 bands cannot be separated and only one broad band occurs at  $\sim$ 1,600-cm<sup>-1</sup>.

The second-order region (2,200–3,400 cm<sup>-1</sup>) shows several features at  $\sim$ 2,400,  $\sim$ 2,700,  $\sim$ 2,900 and  $\sim$ 3,300-cm<sup>-1</sup>, attributed to overtone or combination scattering (Nemanich and Solin 1979). The most important band, near 2,700-cm<sup>-1</sup> (S1 band), splits into two bands in well crystallized graphite. From Lespade et al. (1984), this splitting occurs when CM acquires a triperiodic order. In this study, we focussed on the 2,700–2,900-cm<sup>-1</sup> region in order to check the appearance of this characteristic structure.

### High resolution transmission electron microscopy (HRTEM)

HRTEM investigations were performed using a Philips CM20 microscope working at 200 kV, giving a resolution of 0.144 nm in lattice fringes. CM usually exhibits a multiscale organization. At the atomic scale (structure), CM is made of polyaromatic layers of nanometric dimensions, most of them are stacked to form BSU (Franklin 1951; Oberlin 1989). The mutual orientation in space of these layers from the nanometre to the micrometre scales corresponds to the carbon microtexture. The microtexture can be directly imaged using TEM by coupling various modes (Oberlin 1989; Rouzaud and Oberlin 1989). The CM multiscale organization, thus, is the fingerprint for the CM precursor and conditions of formation. In this study, we mainly used bright-field mode (BF) with a magnification of  $\sim$ 50,000 $\times$  and a high-resolution mode with a magnification of  $\sim$ 300,000 $\times$ . Thanks to the 002 lattice fringe technique (002LF) it is possible to directly image the profile of the aromatic layers. By using this method it is possible to have a direct measurement of (1) the diameter of coherent domains  $L_a$  (i.e. corresponding to the layers stacked and responsible for the presence of the 002 ring in the SAED pattern) and (2) the number of stacked layers ( $N$ ). Moreover, by coupling high-resolution mode with low-magnification bright-field images, TEM is useful in specifying the sample heterogeneity from the nanometre to the micrometre scale. We have coupled these images with selected area diffraction patterns (SAED) to specify the crystallinity range of the sample and especially to follow the occurrence of the triperiodic order. These SAED were obtained on volumes of less than 1  $\mu$ m in diameter and 0.1  $\mu$ m in thickness.

The turbostratic carbons, which have a biperiodic order structure, are characterized by the presence of broad  $hk$  bands in their SAED patterns. In contrast, triperiodic graphite lamellae are

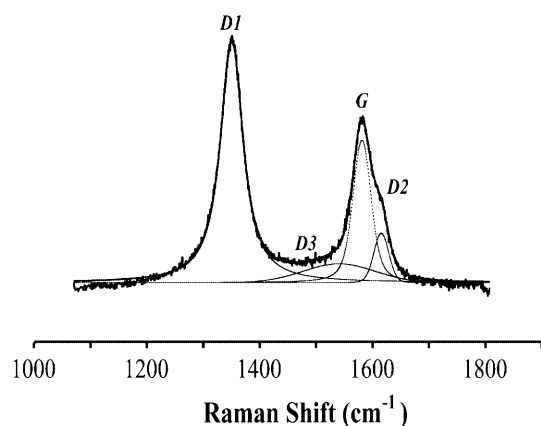


**Fig. 3.** Example of decomposition of the first-order region of the Raman spectrum (sample 5)

characterized by  $hk0$  reflections (100 and 110) when lying on their 001 basal plane and  $hkl$  (100, 101, 110 and 112) and  $00l$  (002, 004, ...) reflections in the folded area. At last, partially graphitized carbons give modulations of both 10 and 11 bands instead of the corresponding  $hkl$  reflections in addition to the  $00l$  reflections present only in folded areas. Nevertheless, it is difficult to assess more precisely the graphitization degree from SAED patterns because the intensity of  $hkl$  reflections is strongly dependent on the orientation of the sample relative to the electron beam.

## Results

### Quantification of the graphitization process by Raman microspectroscopy

Figure 4 shows first- and second-order regions of representative spectra along the cross section. In the first-order region, the general shape of the spectrum can be used as a good metamorphic-grade indicator (Pasteris and Wopenka 1991; Wopenka and Pasteris 1993). From west to east, the following features are evidence for the general increase in metamorphic grade. The first feature is the decrease in the relative intensity and area of the D1 band. This band, which is large and intense in sample 1, decreases along the section and appears to be narrow in the highest-grade samples (nos. 11 and 12). The D3 band, which is very wide in the lowest-grade samples, decreases and is absent from sample 7 onwards. In the poorly organized sample from Fraiteve Mount (sample 1), the G band appears as a wide band occurring near  $1,600\text{ cm}^{-1}$ . In this sample, it was impossible to separate the contributions of the D2 component from that of the G band. From sample 2 onwards, this wide band splits into the two expected bands and then the D2 component decreases with increasing metamorphic grade whereas the G band becomes sharper and sharper (Fig. 4). Thus at the Raman scale, sample 1 appears as poorly organized in comparison with the others. Its spectrum is similar to the spectra obtained from meta-anthracites (Wopenka and Pasteris 1993). In the second-order spectrum, the S1 band is the main spectral feature (Fig. 4). In poorly organized CM from Fraiteve, the

second-order spectrum ( $2,500\text{--}3,000\text{ cm}^{-1}$ ) presents two broad bands of  $\sim 2,700$  and  $\sim 2,900\text{ cm}^{-1}$ . With increasing metamorphic grade, the S1 band increases relatively to the S2 band, and becomes asymmetric in the higher-grade samples indicating a subsequent splitting (samples 11 and 12). The S2 band decreases and disappears almost totally in the highest-grade sample (Finestre pass, sample 12).

We have also checked the influence of strain on the degree of organization of CM in our samples by using Raman microspectroscopy. At the micrometre scale within each thin section, we recorded spectra from CM situated in shear zones and from CM that was diffuse in the foliation. We did the same comparison between CM in very sheared samples located in a major shear zone at the metre scale, and samples from the least deformed zones. In each case, no significant variations were observed and, consequently, the influence of shear on graphitization is not evident within these samples, probably because all the samples are foliated.

In order to quantify these observations, we performed decompositions of spectra using conventional fitting methods. The profile used for each band is a Voigt function. Results are presented in Fig. 5, which shows the G band position, G band FWHM, D1/G intensity ratio and D1/(G + D1 + D2) area ratio (integrated area). Error is given as the standard deviation ( $\pm 1\sigma$ ) from the mean calculated by considering all spectra obtained within a same sample. Heterogeneity within a sample is noticeable in each of these parameters and is more important in lower-grade samples. However, despite the large heterogeneity, the general evolution of all of these parameters is significant (Fig. 5). With increasing metamorphic grade from west to east, the G band shifts from  $\sim 1,590$  to  $1,580\text{ cm}^{-1}$  and becomes progressively narrower (from  $\sim 55\text{ cm}^{-1}$  in sample 1 to  $\sim 20\text{ cm}^{-1}$  in sample 12). At the same time, the relative contribution of the D1 band decreases as shown by both the decrease of the D1/G intensity ratio and of the D1/(G + D1 + D2) area ratio.

An interesting point is the comparison between the respective evolutions of the D1/G intensity ratio and D1/(G + D1 + D2) area ratio along the section. The evolution of the D1/G intensity ratio shows a maximum for sample 3, whereas the D1/(G + D1 + D2) area ratio decreases from samples 1 to 12. Indeed, in the lowest-grade samples (nos 1–2), the D1 band appears as a very wide band, but with a low relative intensity. A similar evolution was previously observed by Bény-Bassez and Rouzaud (1985) in the characterization of the D1/G intensity ratio obtained by studying the graphitization of synthetic cokes under a purely thermal effect. Such an artefact is not observed in the evolution of the D1/(G + D1 + D2) area ratio, which is more continuous and, thus, we think that the latter parameter is the most reliable one to follow the graphitization process. The evolution of this ratio shows a rather constant value of  $\sim 0.6\text{--}0.7$  in the first part of the section between samples 1 and 7, whereas in the second part the ratio progressively decreases from  $\sim 0.6$  to  $\sim 0.3$ .

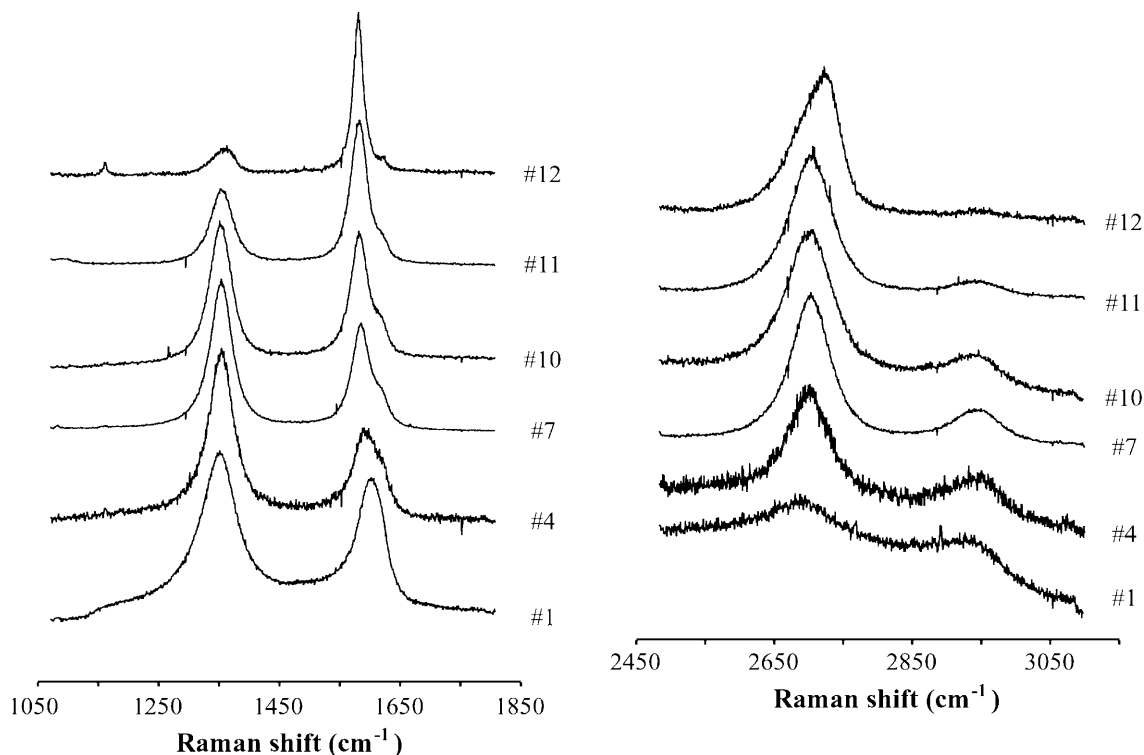


**Fig. 4.** First- and corresponding second-order regions of selected Raman spectra along the cross section. Spectra are *numbered* according to the sample position along the cross section

#### Characterization by HRTEM

In the Fraiteve sample (no 1), CM occurs as a poorly organized material presenting both concentric microtextures (onion rings) and microporous microtextures (Fig. 6a, b, respectively). In this sample, the diameter of the onion rings ranges from 20 and 40 nm (Fig. 6a) whereas the pore diameter is around a few nanometres (Fig. 6b). In the two types of microtextures, the diameter of the coherent domains is lower than 10 nm. In sample 1, but also in all other samples of the cross section, the heterogeneity of organisation for each type of CM is large, but it is almost impossible to quantify it at the HRTEM scale. Moreover, the HRTEM investigations did not allow us to estimate the relative proportions of the onion-ring-like and microporous phases. However, both are widely present in all samples investigated, whatever the metamorphic grade.

Figure 7 is a 002LF image obtained from sample 5 showing an onion ring trapped in a microporous matrix. This clearly shows that the two types of starting materials are intimately interconnected and that their microtextures are clearly associated. At last, it is important to note that in all the samples investigated, neither truly amorphous carbon phases were found because the 002 ring is always present in the SAED patterns as well as two or three parallel fringes in the 002LF images.

#### Evolution of the onion-ring-like CM with increasing metamorphic grade

As shown in Fig. 8, both the microtexture and structure of onion rings are considerably modified with increasing metamorphic grade along the geological cross section. In the western part of the section (samples 1–7), the rings' diameter are more or less constant between 20 and 60 nm. From samples 1–7, the aromatic layers reorient themselves and become longer, especially at the outer part of the rings where the radius of curvature is maximum. Consequently, the diameter of the coherent domains increases as does the number of stacked layers. These transformations are represented by samples 4 and 5 in Fig. 8a, b, respectively, with sample 5 showing a higher degree of organization. In some of the samples (nos. 4–7), some of the rings exhibit a larger diameter of up to 150 nm and then graphitization is promoted by these larger diameters (Fig. 8c). From samples 1–7, the stacking and increase in diameter of coherent domains progresses radially from the outer part towards the centre of the rings, which remains poorly organized.

In the higher grade samples of the eastern part of the section (samples 8–12), the final stages of graphitization of these structures are characterized by a decohesion of the well-crystallized wall from the internal core of the structure, which is still distinguished by a poor structural organization (Fig. 8d, from sample 7). This decohesion is made easier by the formation of edges along the walls, implying a polygonization of the ring structures (Fig. 8e, from sample 8). With this rupture of the detached walls, stiffening of the aromatic planes can be achieved, a triperiodic order can develop and the subsequent

formation of graphitic lamellae can then occur. On the other hand, the core remains poorly organized and the contrast of organization between the two parts can be at the origin of the structural heterogeneity of these samples. In the highest-grade sample, graphitic lamellae are the dominant phase and it is then difficult to separate the respective evolutions of the onion rings and the microporous microtextures (Fig. 9).

#### Evolution of the microporous CM with increasing metamorphic grade

The evolution of the microporous phase with increasing metamorphic grade also shows significant features (Fig. 10). The most spectacular is the increase in pore diameter from a few nanometres in sample 1 to  $> 100$  nm in the highest-grade samples. On the western part of the cross section (samples 2–7), the microtextural organization of this type of CM is composed of both micropores and mesopores, with diameters ranging from a few nanometres up to 10–20 nm. With the increase in pore diameter, the number of stacked layers increases whereas the layers become longer and up to a few tens nanometres, but remain distorted. In this part of the section, which corresponds to a lower degree of metamorphism, the pore diameter and therefore the subsequent degree of organization of CM increase from samples 2 to 7. These transformations are illustrated in Fig. 10a, which is obtained from sample 5.

From sample 7 onwards, the mesopores are progressively transformed into macropores with diameter of several tens nanometres and thick walls (Fig. 10b). As the aromatic layers are more or less continuous along the walls, the diameter of the coherent domains can then reach hundreds of nanometres in value. Generally, the pores are not concentric, but asymmetric and locally flattened along a preferential direction. In the highest grade sample, it is difficult to distinguish the real pore walls from the graphitic lamellae (Fig. 10c, from sample 11). Indeed, the final stage corresponds to a rupture of pore walls along edges, as indicated by the arrow in Fig. 10b. These edges are similar to those responsible for the decohesion of onion-ring structures.

#### Structural evolution (SAED)

Structural analyses obtained by SAED are presented in Fig. 11. Because the two types of CM are intimately mixed, and because the surface sampled in the SAED pattern is around  $1 \mu\text{m}^2$ , SAED patterns correspond to a mixture of both types of CM. Starting material from Fraitveve (sample 1) is turbostratic with only  $hk$  bands visible and no modulations (Fig. 11a). As these  $hk$  bands are large on the SAED pattern, we can conclude that domains are small and misorientated, which is in agreement with 002LF and BF images observations. In sample 5, CM remains turbostratic, but the general thinning of  $hk$

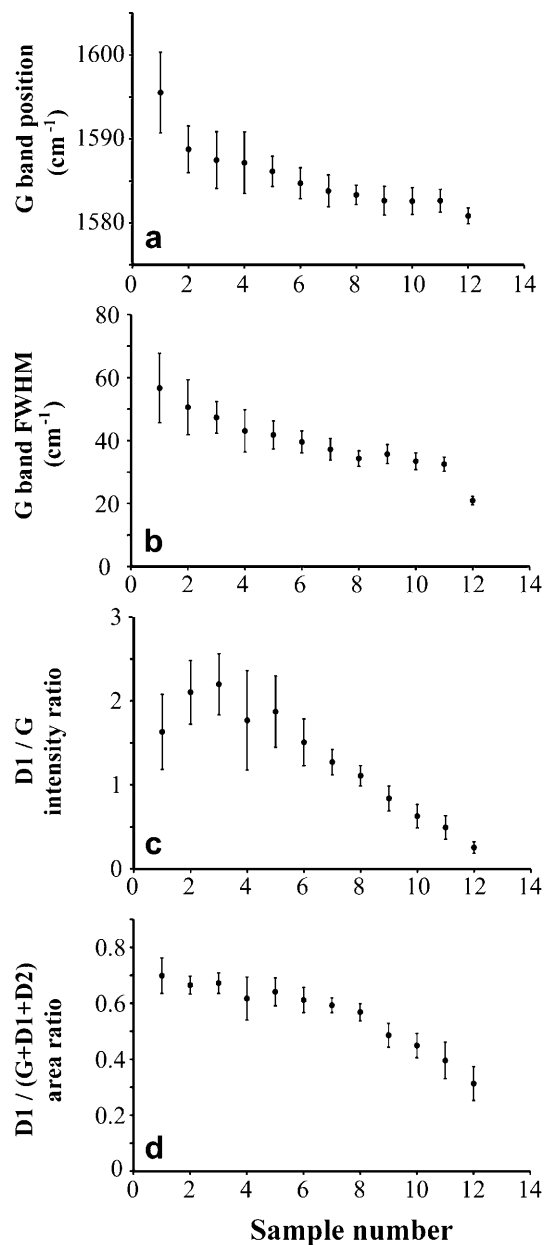
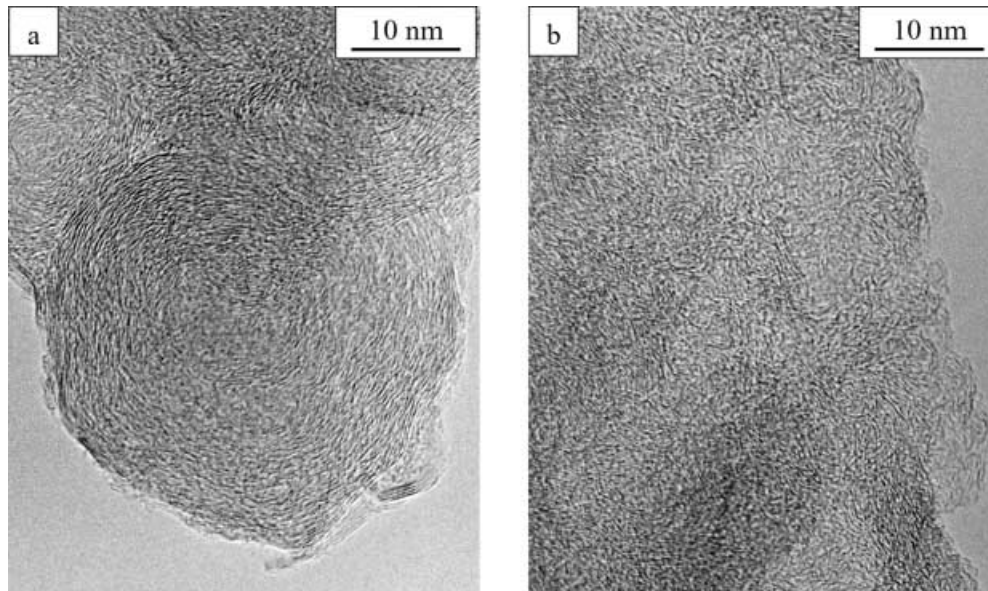


**Fig. 5a–d.** Results of decomposition of Raman spectra along the cross section. **a** Position of the G band, **b** G band full width at half maximum (FWHM), **c** D1/G band intensity ratio, **d** D1/(G+D1+D2) band area ratio

bands shows an increase in the domain dimensions (Fig. 11b). In sample 8, punctuations of bands indicate the presence of large domains and modulations of 11 bands (110 and 112 reflections) can be observed (Fig. 11c). This SAED pattern corresponds to a partially graphitized macroporous phase. This phase is characterized by a preferential orientation (002 arc), which could correspond to pore flattening. In the high-grade sample 11, triperiodic graphite locally occurs (Fig. 11d). It is important to note that no single crystal was observed by using the SAED in all samples investigated. Consequently, the crystallite size in all of these samples is smaller than  $1 \mu\text{m}$ .

**Fig. 6a,b.** HRTEM pictures from sample 1. **a** 002 lattice fringes image of onion ring microtexture from the Fraiteve sample 1 with a diameter of about 40 nm. The core is poorly organized in comparison with the outer part. **b** 002 lattice fringes image of microporous poorly organized CM from sample 1. Both the pores diameter and  $L_a$  are around a few nanometres



## Discussion

The degree of organization of CM as an indicator of HP–LT metamorphism

Both Raman spectroscopy and HRTEM investigations show that the degree of organization of CM is a sensitive indicator of HP–LT metamorphic grade along the studied cross section in the Schistes Lustrés unit. Along this cross section an onion-ring like CM and a microporous CM are progressively transformed into triperiodic graphite with an increase in P–T conditions. The evolution of the  $D1/(G+D1+D2)$  area ratio along the section should be compared with the evolution of both pressure and temperature along the section. Indeed, this ratio is quasi-constant around  $\sim 0.6$ – $0.7$  in the first part of the section (samples 1–7), corresponding mainly to an increase in pressure (from  $\sim 13$  kbar at  $\sim 330$  °C to  $\sim 19$  kbar at  $\sim 370$  °C) whereas it decreases progressively from  $\sim 0.6$  to  $\sim 0.3$  in the second part (samples 8–12), corresponding mainly to an increase in temperature (from  $\sim 19$  kbar at  $\sim 370$  °C to  $\sim 20$  kbar at  $\sim 500$  °C). As the main decrease of the  $D1/(G+D1+D2)$  area ratio is localized where the main variation of temperature occurs, the degree of organization of CM appears to be very sensitive to variations in temperature, even in a HP–LT gradient.

This assumption is confirmed by the results of the HRTEM investigation. The first part of the section (samples 1–7) is indeed characterized by a general enhancement of the degree of organization of CM with an increase of both  $L_a$  and  $N$  parameters. Nevertheless, in these samples there is no spectacular evolution of the microtexture in the sense that the textures observed in sample 1 (onion rings, micropores) are preserved and slightly modified up to sample 7. In contrast, the second

part of the section (samples 7–12) shows spectacular modifications with the disappearance of both the rings and the pores, and the subsequent apparition of graphitic lamellae.

It is interesting to note that the results obtained by Raman spectroscopy are in very good agreement with those of the HRTEM investigations. The two methods show the same general trend in the evolution, and, thus, Raman spectroscopy completes HRTEM investigations by giving quantitative parameters on the degree of organization of CM. At both nanometre and micrometre scales, the graphitization appears as a progressive and continuous process along the studied cross section. Bény-Bassez and Rouzaud (1985) have established correlations between the  $L_a$  values estimated from HRTEM pictures and various parameters

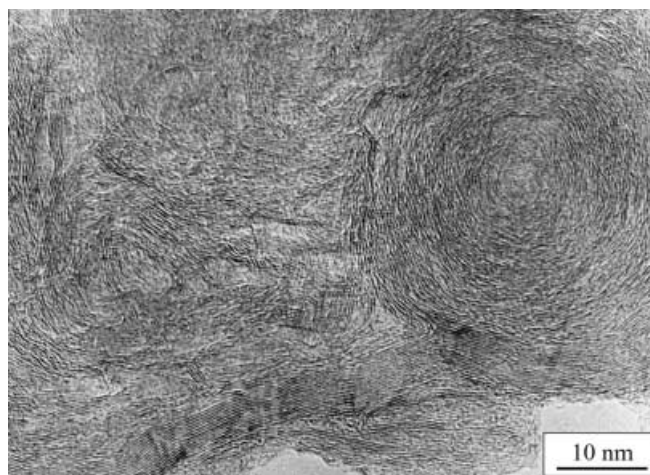
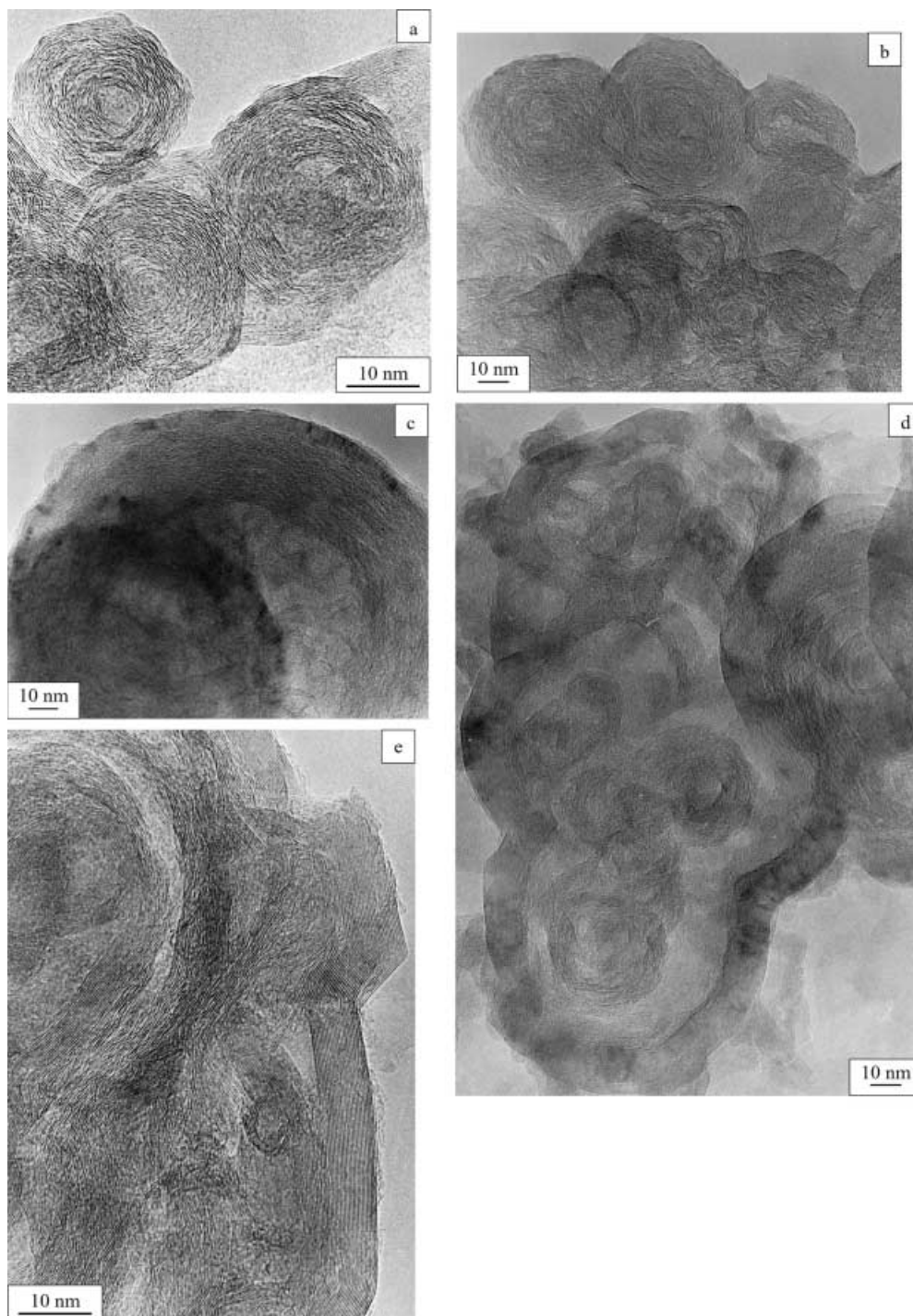


**Fig. 7.** 002 lattice fringe image from sample 5 showing the coexistence of onion ring (*right*) and microporous (*left*) microtextures. This kind of association between the two phases was found in all the samples investigated, with a degree of organization for each phase varying with the metamorphic grade

**Fig. 8a–e.** HRTEM images of progressive graphitization of onion-rings concentric microtextures along the cross section. **a, b** 002 lattice fringes image of onion-ring structures from samples 4 and 5, respectively. The aromatic layers are long and planar in the outer part whereas the core is characterized by short and misorientated layers. **c** (Low magnification) Large onion-ring structure from sample 4 with a diameter of  $\sim 100\text{--}150$  nm. The border of the structure consists of distorted stacked layers whereas the interior remains poorly organized. **d** (Low magnification) Decoherence of the outer part of onion-rings microtextures from the poorly organized core in sample 7. **e** 002 lattice fringes image showing the rupture of the outer wall (indicated by the *arrow*) and subsequent decohesion from the core in sample 8



from the Raman spectrum (FWHM, intensity and area ratio for instance) obtained from various synthetic CM. Such correlations are impossible to achieve within our heterogeneous samples. The complementarity between HRTEM and Raman microspectroscopy is well illustrated by the detection of the apparition of the triperiodic order along the Schistes Lustrés cross section: both the modulation of  $hk$  bands in the SAED pattern and the splitting of the S1 Raman bands appear in the same samples – nos 11 and 12. Moreover,

as it was not possible to detect by SAED the presence of single crystal of graphite in the higher grade samples; the size of crystallites within these samples can be considered to be smaller than a micron. This result is in good agreement with the presence of a D1 band within all the spectra analysed in this study. As the area sampled by the Raman microprobe is around a few square microns, the defects concentrated at the grains boundaries are responsible for the remaining D1 band.



**Fig. 9.** 002LF image of perfectly stacked aromatic layers in a graphite flake from sample 12. It is impossible to distinguish if such a graphitic lamella derives from the evolution of the microporous phase or from the onion-ring like phase

### The influence of metamorphic gradient on the graphitization process

This work is the first study of natural graphitization along a homogeneous section that combines Raman spectroscopy and HRTEM. Nevertheless, Buseck and Huang (1985) and Wopenka and Pasteris (1993) have studied the same samples from the HT–LP metamorphic series of the Narragansett basin (USA) by HRTEM and Raman spectroscopy, respectively. Although the authors have noticed a heterogeneity within the type of CM precursor and that some samples have experienced two major phases of metamorphism (Wopenka and Pasteris 1993), it is interesting to compare some of their observations with our results.

If we compare the  $D1/(G+D1)$  area ratio obtained by Wopenka and Pasteris (1993), considering that the contribution of the D2 band is very low, and the values of the  $D1/(G+D1+D2)$  area ratio obtained in our samples, we can see that the ratio they observed in the chlorite ( $\sim 0.5$ – $0.6$ ) and the garnet ( $\sim 0.3$ ) zones are similar to the ratio estimated in our samples in the lower-grade and higher-grade samples, respectively. Moreover, the general modifications of organization of CM observed by Buseck and Huang (1985) with increasing metamorphic grade seem to be comparable with the succession of stages described above in our samples. They observed a microporous-like CM in the chlorite zone, a macroporous-like CM in the chlorite/biotite and garnet zones and graphitic lamellae in the higher grade part of the garnet zone and in the sillimanite zone. Thus, in HP–LT and HT–LP metamorphic gradients, graphitization seems to proceed by the same mechanism and succession of stages. For instance, at the same temperature, Raman spectra and microtextural organization seem to be similar whatever the pressure. This assumption has to be confirmed by the systematic study of the degree of organization of CM along a reference cross section with a homogeneous precursor and well quantified HT–LP metamorphic evolution.

### Problems of heterogeneity within CM structure and microtexture

In all the samples of the Schistes Lustrés cross section, CM is strongly structurally and microtexturally heterogeneous. As previously shown by Kribek et al. (1994) and Large et al. (1994), one of the main problems in the study of natural graphitization is to deal with the strong heterogeneity of CM structure and microtexture. Structural and microtextural heterogeneity of CM can have various origins, such as heterogeneity within the carbon precursor (Bény-Bassez and Rouzaud 1985; Kribek et al. 1994; Large et al. 1994) or anisotropy in the repartition of stresses (Kamiya et al. 1973; Bustin et al. 1995).

For instance, nanometre-scale heterogeneity within our samples is primarily caused by the presence of two types of CM precursors, which are microtexturally different: onion-ring concentric microtextures and microporous carbons. The structure and microtexture of the microporous CM are very similar to those described in saccharose-based cokes or meta-anthracites (Rouzaud and Oberlin 1989; Rouzaud and Oberlin 1990). The onion-ring type was described by Buseck and Huang (1985) and Deurbergue et al. (1987) and seems to be common in CM from low-grade metasediments of a marine origin. These concentric microtextures are very similar to carbon black produced by thermal decomposition of hydrocarbons. As the host-rock origin is supposed to be a marine sediment, the two types of CM precursors observed within our samples could be derived from an algae kerogen for the microporous part and a hydrocarbon fraction for the concentric microtextures (e.g. Ayache 1987). Such a hydrocarbon phase should have been released during diagenesis, but may have remained trapped because of the impermeability of the sediments.

Two types of CM have been recognized in all samples, but, however, with difficulty in the higher-grade samples (nos. 11 and 12) where CM occurs mainly as graphitic lamellae. When looking at one type of CM, there is also a strong heterogeneity in the observed microtexture. As we have seen in the case of the onion rings, this heterogeneity is caused by the mechanism of graphitization itself, which produces graphitic lamellae from the outer part of the rings, but preserves the poorly organized cores at the same time. However, in all samples presented in this work, a large part of the CM is transformed to the expected grade whereas a minor fraction remains poorly organized and, more rarely, untransformed.

At the Raman micrometre scale, heterogeneity within each sample is also very strong, but we were not able to distinguish between the various causes of this heterogeneity: type of CM or pressure effects at grains boundaries for instance. However, whereas purely thermally treated cokes seem to be homogeneous (Bény-Bassez and Rouzaud 1985), heterogeneity within our sample seems to be less important than heterogeneity within

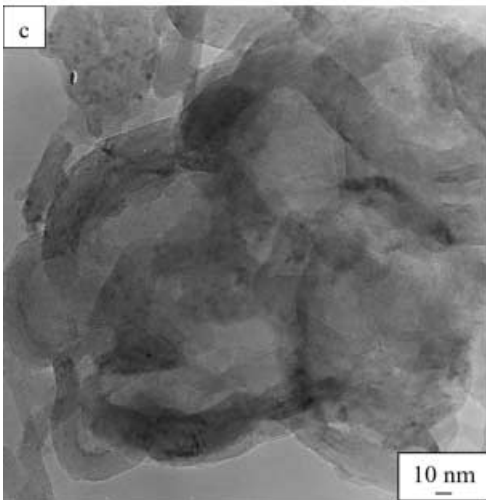
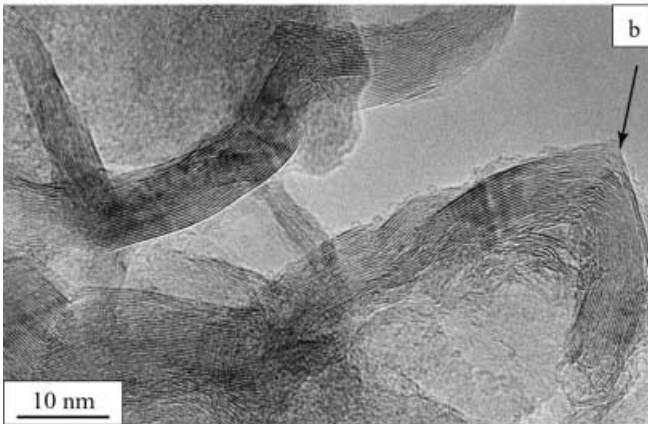
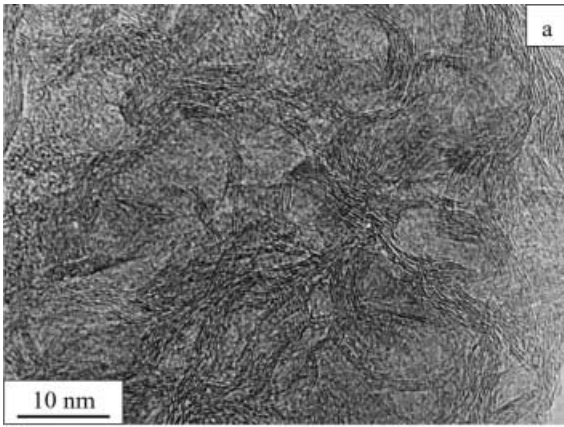


**Fig. 10a–c.** HRTEM images of progressive graphitization of microporous CM along the cross section. **a** (002LF) Mesoporous CM from sample 5. In comparison with Fig. 6a, note the increase in micropore diameter,  $L_a$ , and number of stacked layers. **b** (002LF) Macroporous CM from sample 8. The *arrow* indicates the edge along which the pore wall preferentially breaks. **c** (Low magnification) Macroporous CM from sample 11. Note the large pore diameters up to a 100 nm and the thickness of the walls

CM experimentally heat-treated under pressure (Bustin et al. 1995; Beyssac et al. 2000). Moreover, it is also generally accepted that graphitization proceeds further

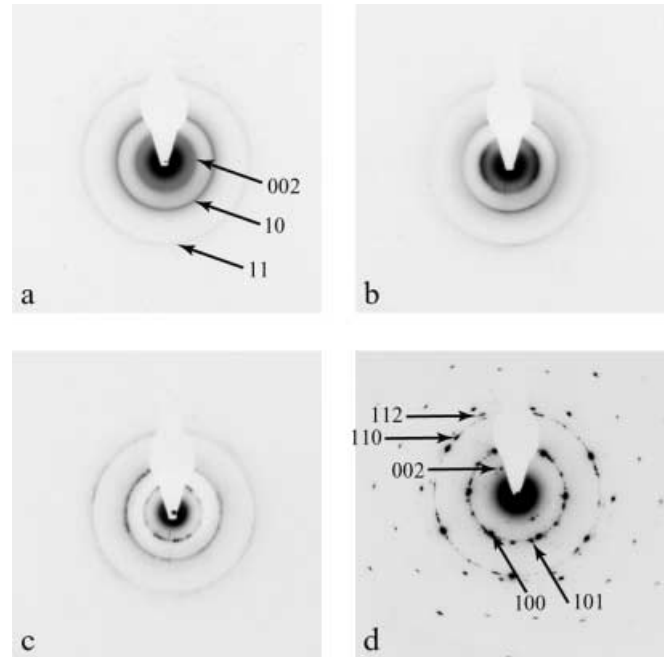


**Fig. 11a–d.** Evolution of the SAED pattern of CM with increasing metamorphic grade along the cross section. **a** Sample 1; **b** sample 5; **c** sample 8, **d** sample 11

in regional metamorphism than in contact aureoles, especially at temperatures lower than 550–600 °C (Wada et al. 1994). These considerations raise the problem of the initiation of graphitization under pressure and the eventual kinetic controls on this process.

#### Implications for the study of the mechanisms of graphitization

On the basis of our HRTEM investigations we propose a mechanism of graphitization of CM submitted to regional metamorphism. Firstly, it is important to note that microporous CM and onion-ring structures are non graphitizing carbons under the effect of temperature at ambient pressure, even as high as 2,800 °C: for instance, under the pure effect of temperature, the microtexture of the microporous CM is hardly modified (Rouzaud and Oberlin 1989). As a consequence, the graphitization of onion-ring structures as well as microporous CM implies microtextural modifications that are induced by pressure. In the two cases, the final stage is constituted by a rupture of these microtextures, which produces graphitic lamellae.

This mechanism should be compared with those proposed by de Fonton et al. (1980) and Bustin et al. (1995). By studying with HRTEM and XRD, the graphitization process of hard carbons (glassy carbon and sugar-based coke) submitted to high-pressure and high-temperature experiments, de Fonton et al. (1980) have proposed the existence of a new carbon phase that is texturally and structurally macroporous and turbostratic. They suggest that this macroporous phase results

from the coalescence of micropores in the starting material under the effect of pressure. Moreover, according to these authors, the graphitization of such macroporous phase is caused by a breaking of pore walls as a consequence of the stress and shear pressure that develop in a porous phase submitted to hydrostatic pressure. As they did not detect the presence of intermediate stages between microporous starting materials, macroporous phases and graphitic lamellae, the authors interpreted this macroporous phase as a new carbon phase. This macroporous carbon phase has been also described in natural samples (Bonijoly et al. 1982; Deurbergue et al. 1987). In both experimental and natural graphitization, these authors described the graphitization process as non-progressive because of drastic microtextural changes during the process.

In contrast, the evolution of the different Raman parameters is relatively progressive and continuous with increasing metamorphic grade along the Schistes Lustrés unit. Moreover, we have detected numerous intermediate stages by HRTEM between microporous, macroporous, and graphite stages: the dewrinkling and joining of the turbostratic sheets to form long-range ordered layers is progressive with increasing metamorphic grade. As a consequence, the graphitization along the Schistes Lustrés cross section seems to be a progressive and continuous process, which proceeds heterogeneously at the nanometre scale. The role of pressure in such a process is fundamental because pressure induces the microtextural changes that are necessary for the organizational modifications of CM, and thus for graphitization. In our study, the sampling was systematic and homogeneously distributed along the section, whereas Bonijoly et al. (1982) and Deurbergue et al. (1987) worked with dispersed samples from various origins without progressive evolution of the metamorphic grade. As a consequence, we assume that the graphitization caused by regional HP–LT metamorphism is progressive and continuous, as has been demonstrated in a HT–LP context (Buseck and Huang 1985; Wopenka and Pasteris 1993). In such a process, the macroporous microtexture has to be considered as a transitional stage, but in any case it should be considered as a new carbon phase.

**Acknowledgements** This work was supported by the CNRS – programme matériaux (projet 114) and by the INSU – programme géomatériaux. We would like to thank P. Gillet for access to the Raman spectroscopy facilities (ENS Lyon). We warmly thank J. Cassareuil for the quality of the thin sections and C. Clinard, T. Cacciaguera, N. Catel and G. Montagnac for their help. Comments by J. Dubessy and two anonymous reviewers greatly improved this manuscript. Lastly, we acknowledge the helpful editorial work of J. Hoefs.

## References

- Agard P, Jolivet L, Goffé B (2001a) Tectonometamorphic evolution of the Schistes lustrés complex: implications for the exhumation of HP and UHP rocks in the western Alps. *Bull Soc Geol Fr* 172(5):617–636
- Agard P, Vidal O, Goffé B (2001b) Interlayer and Si content of phengite in HP–LT carpholite-bearing metapelites. *J Metamorph Geol* 19(5):479–496
- Ayache J (1987) Simulations thermiques de l'évolution des roches mères pétrolières. Pyrolyses de substances modèles. PhD Thesis, University of Orléans, Orléans
- Barfety JC, Lemoine M, Graciansky PC, Tricart P, Mercier D, with the collaboration of Pêcher A, Bertrand J, Nievergelt P, Amaudric du Chaffaut S, Dumont T, Monjuvent G, Goffé B, Kienast JR, Mével C, Gravost M, Sauret B, Godefroy P (1995) Notice explicative, Carte Géol France (1/50,000), feuille Briangon (823), Orléans
- Bény-Bassez C, Rouzaud JN (1985) Characterization of carbonaceous materials by correlated electron and optical microscopy and Raman microspectroscopy. *Scanning Electron Microsc* 119–132
- Beyssac O, Rouzaud JN, Brunet F, Petit JP, Goffé B (2000) Pressure effects on graphitization: experimental constraints. *J Conf Abstr* 5:13
- Bonijoly M, Oberlin A (1982) A possible mechanism for natural graphite formation. *Int J Coal Geol* 1:283–312
- Buseck PR, Huang BJ (1985) Conversion of carbonaceous material to graphite during metamorphism. *Geochim Cosmochim Acta* 49:2003–2016
- Buseck PR, Huang BJ, Miner B (1988) Structural order and disorder in Precambrian kerogens. *Org Geochem* 12:221–234
- Bustin M, Rouzaud JN, Ross JV (1995) Natural graphitization of anthracite: experimental considerations. *Carbon* 33(5):679–691
- Caron JM (1977) Lithostratigraphie et tectonique des Schistes Lustrés dans les Alpes cottiennes septentrionales et en Corse orientale. PhD Thesis, University of Louis Pasteur, Strasbourg
- De Fonton S, Oberlin A, Inagaki M (1980) Characterization by electron microscopy of carbon phases (intermediate turbostratic phase and graphite) in hard carbons when heat-treated under pressure. *J Mater Sci* 15:909–917
- Deurbergue A, Oberlin A, Oh JH, Rouzaud JN (1987) Graphitization of Korean anthracites as studied by transmission electron microscopy and X-ray diffraction. *Int J Coal Geol* 8:375–393
- Diessel CFK, Brothers NR, Black PM (1978) Coalification and graphitization in high-pressure schists in New Caledonia. *Contrib Mineral Petrol* 68:63–78
- Durand B, Monnin JC (1980) Elemental analysis of kerogens (C, H, O, N, S, Fe). In: Durand B (ed) *Kerogen*. Technip, Paris, pp 113–141
- Ferrari AC, Robertson J (2000) Interpretation of Raman spectra of disordered and amorphous carbon. *Phys Rev B* 61(20):14095–14107
- Franklin RE (1951) The structure of graphitic carbons. *Acta Crystallogr* 4:253–261
- Goffé B, Vilely M (1984) Texture d'un matériel carboné impliqué dans un métamorphisme haute pression-basse température (Alpes françaises). Les hautes pressions influencent-elles la carbonification? *Bull Minér* 107:81–91
- Grew ES (1974) Carbonaceous material in some metamorphic rocks of New England and other areas. *J Geol* 82:50–73
- Itaya T (1981) Carbonaceous material in pelitic schists of the Sambagawa metamorphic belt in central Shikoku, Japan. *Lithos* 14:215–224
- Jehlicka J, Rouzaud JN (1989) Organic geochemistry of Precambrian shales and schists (Bohemian massif, central Europe). *Adv Org Geochem* 16(4–6):865–872
- Jehlicka J, Rouzaud JN (1997) Raman microspectrometry of accumulated non-graphitized bitumens. *J Raman Spectrogr* 28:717–724
- Kamiya K, Inagaki M, Noda T (1973) Oriented heterogeneous graphitization of carbons under high pressure. *High Temp–High Pressure* 5:331–338
- Kovalevski VV, Buseck PR, Cowley JM (2001) Comparison of carbon in shungite rocks to other natural carbons: an X-ray and TEM study. *Carbon* 39:243–256
- Kretz R (1983) Symbols for rock-forming minerals. *Am Mineral* 68:277–279

- Kribek B, Hrabal J, Landais P, Hladikova J (1994) The association of poorly ordered graphite, coke and bitumens in greenschist facies rocks of the Ponickla Group, Lúgicum, Czech Republic: the result of graphitization of various types of carbonaceous matter. *J Metamorph Geol* 12:493–503
- Landis CA (1971) Graphitization of dispersed carbonaceous materials in metamorphic rocks. *Contrib Mineral Petrol* 30:34–45
- Large DJ, Christy AG, Fallick AE (1994) Poorly crystalline carbonaceous matter in high grade metasediments: implications of graphitization and metamorphic fluids compositions. *Contrib Mineral Petrol* 116:108–116
- Lemoine M, Bas T, Arnaud-Vanneau A, Arnaud H, Dumont T, Gidon M, Bourbon M, De Graciansky PC, Rudkiewicz JL, Megard-Galli J, Tricart P (1986) The continental margin of the Mesozoic Tethys in the Western Alps. *Mar Petrol Geol* 3:179–199
- Lespade P, Marchand A, Couzi M, Cruege F (1984) Caractérisation de matériaux carbonés par microspectroscopie Raman. *Carbon* 22:375–385
- Michard A, Goffé B, Chopin C, Henry C (1996) Did the Western Alps develop through an Oman-type stage? The geotectonic setting of high-pressure metamorphism in two contrasting Tethyan transects. *Eclog Geol Helv* 89:43–80
- Mostefaoui S, Perron C, Zinner E, Sagon G (2000) Metal-associated carbon in primitive chondrites: structure, isotopic composition and origin. *Geochim Cosmochim Acta* 64:1945–1964
- Nemanich RJ, Solin SA (1979) First- and second-order Raman scattering from finite-size crystals of graphite. *Phys Rev B* 20(2):392–401
- Nishimura Y, Coombs DS, Landis CA, Itaya T (2000) Continuous metamorphic gradient documented by graphitization and K–Ar age, southeast Otago, New Zealand. *Am Mineral* 84(11–12):1625–1636
- Oberlin A (1989) High-resolution TEM studies of carbonization and graphitization. In: Thrower PA (ed) *Chemistry and physics of carbon*, vol 22. Marcel Dekker, New York, pp 1–143
- Okuyama-Kusunose Y, Itaya T (1987) Metamorphism of carbonaceous material in the Tono contact aureole, Kitakami Mountains, Japan. *J Metamorph Geol* 5:121–139
- Pasteris JD (1989) In situ analysis in geological thin-sections by laser Raman microprobe microspectroscopy: a cautionary note. *Appl Spectrosc* 43:567–570
- Rouzaud JN, Oberlin A (1989) Structure, microtexture, and optical properties of anthracene and saccharose-based carbons. *Carbon* 27(4):517–529
- Rouzaud JN, Oberlin A (1990) The characterization of coals and cokes by transmission electron microscopy. In: Charcosset H, Nickel-Pepin-Donat (eds) *Advanced methodologies in coal characterization*. Elsevier, Amsterdam, pp 311–355
- Pasteris JD, Wopenka B (1991) Raman spectra of graphite as indicators of degree of metamorphism. *Can Mineral* 29:1–9
- Salver-Disma F, Tarascon JM, Clinard C, Rouzaud JN (1999) Transmission electron microscopy studies on carbon materials prepared by mechanical milling. *Carbon* 37:1941–1959
- Stampfli GM, Marchant RH (1997) Geodynamic evolution of the Tethyan margins of the Western Alps. In: Pfiffner OA, Lehner P, Heitzmann P, Mueller S, Steck A (eds) *Deep structure of the Swiss Alps: results of NRP-20*. Birkhauser, Basel, pp 223–239
- Suchy V, Frey M, Wolf M (1997) Vitrinite reflectance and shear-induced graphitization in orogenic belts: a case study from the Kandersteg area, Helvetic Alps, Switzerland. *Int J Coal Geol* 34:1–20
- Tuinstra, F, Koenig JL (1970) Raman spectrum of graphite. *J Chem Phys* 53:1126–1130
- Wada H, Tomita T, Matsuura K, Iuchi K, Ito M, Morikiyo T (1994) Graphitization of carbonaceous matter during metamorphism with references to carbonate and pelitic rocks of contact and regional metamorphisms, Japan. *Contrib Mineral Petrol* 118:217–228
- Wang A, Dhamelincourt P, Dubessy J, Guerard D, Landais P, Lelaurain M (1989) Characterization of graphite alteration in an uranium deposit by micro-Raman spectroscopy, X-ray diffraction, transmission electron microscopy and scanning electron microscopy. *Carbon* 27(2):209–218
- Wang GF (1989) Carbonaceous material in the Ryoke metamorphic rocks. *Lithos* 22:305–316
- Wopenka B, Pasteris JD (1993) Structural characterization of kerogens to granulite-facies graphite: applicability of Raman microprobe spectroscopy. *Am Mineral* 78:533–557
- Yui TF, Huang E, Xu J (1996) Raman spectrum of carbonaceous material: a possible metamorphic grade indicator for low-grade metamorphic rocks. *J Metamorph Geol* 14:115–124